Plasmonics (2022) 17:1681–1689
https://doi.org/10.1007/s11468-022-01655-2

Fano Resonance in the Plasmonic Structure of MIM Waveguide with r-Shaped Resonator for Refractive Index Sensor

Siti Rohimah[1] · He Tian[1] · Jinfang Wang[2] · Jianfeng Chen[1] · Jina Li[1] · Xing Liu[1] · Jingang Cui[1] · Qiang Xu[1] · Yu Hao[3]

Received: 19 December 2021 / Accepted: 5 May 2022 / Published online: 23 May 2022

Abstract

A plasmonic structure of metal–insulator-metal (MIM) waveguide consisting of a baffle waveguide and an r-shaped resonator is designed to produce Fano resonances. The finite element method is used to analyze the transmission characteristics and magnetic field distributions of the plasmonic structure. The simulation results show that two Fano resonances can be achieved by the interference between a continuum state in the baffle waveguide and a discrete state in the r-shaped resonator. The Fano resonances can be tuned by changing the geometrical parameters of the plasmonic structure. The refractive index sensing is investigated and it is found that the sensitivity is strongly dependent on the geometrical parameters. The maximum sensitivity is 1333 nm/RIU, with the figure of merit of 5876. The results of the designed plasmonic structure offer high sensitivity and nano-scale integration, which are beneficial to nano-scale refractive index sensors, biosensors, and photonic devices.

Keywords Surface plasmon polaritons · Fano resonance · r-shaped resonator · Refractive index sensor

Introduction

Surface plasmon polaritons (SPPs), which originate from the interaction of incident photons and free electrons on the metal surface, propagate along with the metal–dielectric interface and have the potential to overcome the light diffraction limit, localization of light in subwavelength, and high level of integration capability [1–3]. SPPs have applications in optical devices such as switches [4, 5], sensors [6–9], integrated photonic devices [10–12], demultiplexers [13], and filters [14, 15]. One of the most promising waveguide structures is the metal–insulator-metal (MIM) waveguide, which has advantages such as low bending loss, simple structure, long propagation distance, deep sub-wavelength confinements, and easy integration [16–20].

Fano resonance is a fundamental resonance phenomenon caused by the interference between a continuum state and a discrete state and has typically sharp resonance peaks and asymmetrical line shapes [21, 22]. Fano resonance can be applied in lasers, slow light devices, and switches [23, 24]. Recently, Fano resonance based on the MIM waveguide structures has been widely studied and applied to sensors. For instance, Wang et al. investigated Fano resonances in a MIM waveguide with a baffle and a circular split-ring resonator cavity and realized the refractive index nanosensor with the maximum sensitivity of 1114.3 nm/RIU [20]. Chen et al. designed a MIM waveguide composed of a circular split-ring resonance cavity and a double symmetric rectangular stub waveguide to generate Fano resonance, and the sensitivity was up to 1180 nm/RIU with the figure of merit (FOM) of 5585.3 [25]. Liu et al. proposed a MIM waveguide structure consisting of a side-coupled rectangular cavity, a rightward opening semi-ring cavity, and a bus waveguide to realize independently tunable Fano resonances, and the sensitivity reached 1550.38 nm/RIU [26].

In this paper, we design a plasmonic structure of MIM waveguide consisting of a baffle waveguide and an r-shaped resonator and discuss its transmission characteristics and magnetic field distributions using the finite element method (FEM). Two Fano resonances are achieved by the interaction between a continuum state in the baffle waveguide and a discrete state in the r-shaped resonator. Then the influences of the geometrical parameters of the structure on the

✉ He Tian
tianhe@nefu.edu.cn

[1] College of Science, Northeast Forestry University, Harbin 150040, China

[2] Shanghai Xin Yue Lian Hui Electronic Technology Co. LTD., Shanghai 200233, China

[3] Jilin Meteorological Information Network Center, Changchun 130062, China

Fano resonances are investigated. Large sensitivity and FOM can be obtained by optimizing the geometrical parameters. Finally, the glucose concentration sensing characteristics of the structure are discussed.

Structural Model

The plasmonic structure of MIM waveguide is shown in Fig. 1, which consists of a single baffle waveguide and an r-shaped resonator. The r-shaped resonator is composed of a rectangular resonator and a quarter-ring resonator. The width W of the bus waveguide and r-shaped resonator is fixed to 50 nm to ensure that only the fundamental transverse magnetic mode exists in the MIM waveguide [27]. The width of the baffle is S, the coupling distance between the bus waveguide and the r-shaped resonator is g, the height of the rectangular resonator is H, and the effective radius of the quarter-ring resonator is defined as $R' = (R + R_0)/2$, where R and R_0 are the outer and inner radii of the quarter-ring resonator.

In Fig. 1, the blue and white areas represent silver and air, respectively. Usually, the relative dielectric constant of air is $\varepsilon_{in} = 1$, and the relative dielectric constant of silver is characterized by the Debye-Drude model [28] :

$$\varepsilon_m = \varepsilon_\infty - \frac{\omega_p^2}{\omega^2 + i\omega\gamma}, \tag{1}$$

where $\varepsilon_\infty = 3.7$ is the dielectric constant at infinite frequency, ω is the angular frequency of incident light in vacuum, $\omega_p = 1.38 \times 10^{16}$ Hz is the bulk plasma frequency of free conduction electrons, and $\gamma = 2.73 \times 10^{13}$ Hz is the electron collision frequency. The fabrication of the plasmonic MIM waveguide structure begins with the preparation of an adequately thick Ag layer on a silicon substrate by using chemical vapor deposition (CVD) [29, 30]. Then, the r-shaped resonator and the bus waveguide can be etched on the Ag layer by electron beam etching.

According to the standing wave theory, constructive interference should occur when the resonance condition is satisfied: $4\pi Re(n_{eff}) l_{eff}/\lambda + \phi = 2m\pi, m = 1, 2, 3, ...$, where l_{eff} is the effective length of the resonator [31–33]. Thus, the resonance wavelength can be derived as:

$$\lambda = \frac{2Re(n_{eff}) l_{eff}}{m - \phi/2\pi}, m = 1, 2, 3, ... \tag{2}$$

where ϕ is the phase shift introduced by the reflection in the resonance resonator, m is the resonant mode order, and $Re(n_{eff})$ is the real part of the effective index n_{eff}.

The two-dimensional FEM is used to analyze the transmission characteristics of the plasmonic structure. We set the perfect matching layers at the top and bottom of the structure to absorb the escaping waves. Light is inputted from Port 1 and then outputted from Port 2. Therefore, the transmittance is expressed as $T = |S_{21}|^2$, where S_{21} is the transmission coefficient from Port 1 to Port 2 [34].

Results and Discussion

In order to investigate the optical properties of the plasmonic structure, the transmission spectra of the single baffle waveguide, the single r-shaped resonator, and the entire structure are numerically calculated and shown in Fig. 2. The geometrical parameters are set as $R = 200$ nm, $R_0 = 150$ nm,

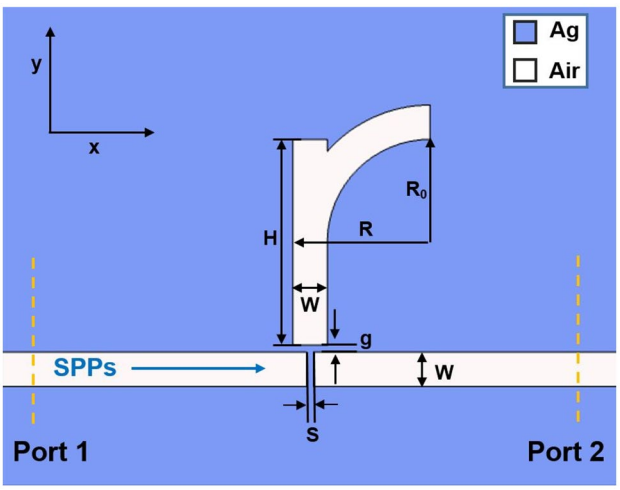

Fig. 1 The schematic and geometrical parameters of the designed plasmonic structure

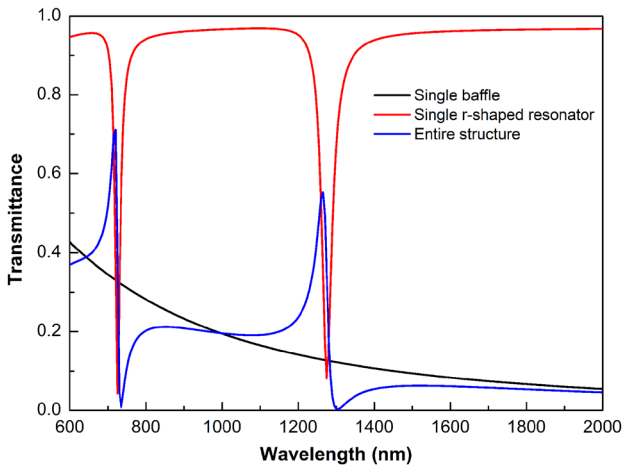

Fig. 2 Transmission spectra of the single baffle waveguide (black line), the single r-shaped resonator (red line), and the entire structure (blue line)

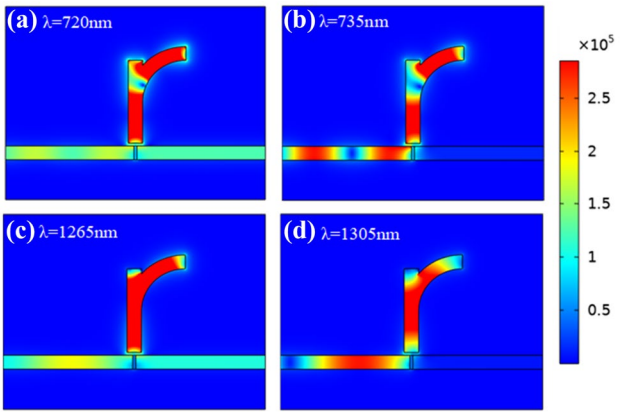

Fig. 3 Magnetic field intensity distributions of the plasmonic structure at **a** $\lambda = 720$ nm (FR_1 peak), **b** $\lambda = 735$ nm (FR_1 dip), **c** $\lambda = 1265$ nm (FR_2 peak), and **d** $\lambda = 1305$ nm (FR_2 dip)

$H = 300$ nm, $S = 10$ nm, and $g = 10$ nm. In Fig. 2, the baffle waveguide produces a continuum state, as indicated by the black line. Meanwhile, the r-shaped resonator coupled with the bus waveguide without the baffle produces a discrete state with two approximately symmetric Lorentzian-like troughs at 725 nm and 1275 nm, described by the red line. As a result, two Fano resonances are obtained by the interference between the continuum state and the discrete state, which are shown by the blue line in Fig. 2. To simplify the discussion, we name the left Fano resonance as FR_1 and the right Fano resonance as FR_2. In order to further investigate the two Fano resonances, the magnetic field intensity distributions of the plasmonic structure at $\lambda = 720$ nm (FR_1 peak), 735 nm (FR_1 dip), 1265 nm (FR_2 peak), and 1305 nm (FR_2 dip) are shown in Fig. 3. In Fig. 3a and c, the magnetic field intensity distributions at Fano resonance peaks are caused by the constructive interference between the continuum state and the discrete state, and the transmission of the structure is enhanced. However, at Fano resonance dips caused by the destructive interference [35], the energy is concentrated in the r-shaped resonator and cannot be transmitted through the structure, as shown in Fig. 3b and d.

The transmission characteristics of the plasmonic structure can be tuned by varying the geometrical parameters. First, we investigate the influences of the coupling distance g and the baffle width S on the Fano resonances. Figure 4a shows the transmission spectra of the structure with different coupling distances. Here, the coupling distance is increased from 5 to 20 nm with an interval of 5 nm, and other parameters are set as $R = 200$ nm, $R_0 = 150$ nm, $H = 300$ nm, and $S = 10$ nm. The increase of the coupling distance produces considerable blueshifts of the two Fano resonance wavelengths. The transmittance of the Fano resonances gradually decreases as the coupling distance increases, because the coupling strength between the r-shaped resonator and the baffle waveguide becomes weak. The relationship between the Fano resonance wavelength and the coupling distance is shown in Fig. 4b. It can be seen that FR_1 and FR_2 make blueshifts from 710 to 730 nm and from 1320 to 1235 nm, respectively. Figure 5a shows the transmission spectra of the plasmonic structure with different baffle widths. The baffle width is increased from 5 to 20 nm with an interval of 5 nm, and other parameters are set as $R = 200$ nm, $R_0 = 150$ nm, $H = 300$ nm, and $g = 10$ nm. With the increase of the baffle width, the line shapes of the Fano resonances become sharper and more symmetric close to Lorentz resonance. As shown in Fig. 5b, the Fano resonance wavelengths hardly change with the baffle width. The resonance wavelengths of FR_1 and

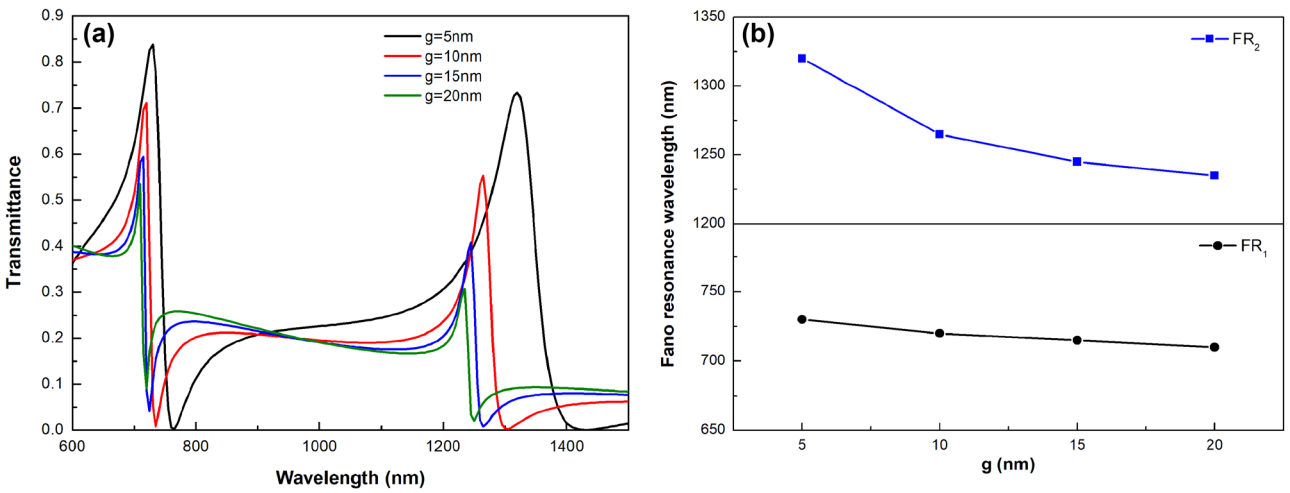

Fig. 4 **a** Transmission spectra of the plasmonic structure with different coupling distances. **b** Relationship between the Fano resonance wavelength and the coupling distance

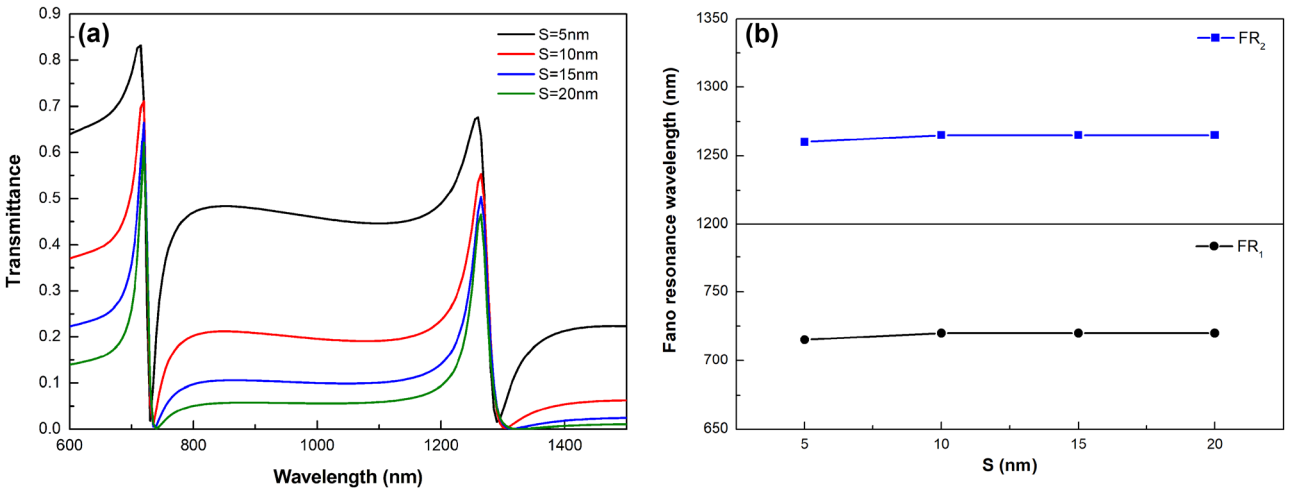

Fig. 5 **a** Transmission spectra of the plasmonic structure with different baffle widths. **b** Relationship between the Fano resonance wavelength and the baffle width

FR_2 change slightly from 715 to 720 nm and from 1260 to 1265 nm, respectively.

Furthermore, the influences of the rectangular resonator height H and the outer radius of the quarter-ring resonator R on transmission spectra are also investigated. In Fig. 6a, the rectangular resonator height is increased from 290 to 320 nm with an interval of 10 nm, and other parameters are set as $R = 200$ nm, $R_0 = 150$ nm, $S = 10$ nm, and $g = 10$ nm. The increase of the rectangular resonator height produces significant redshifts of the Fano resonance wavelengths, and the shift of FR_2 is greater than that of FR_1. Figure 6b shows the relationship between the Fano resonance wavelength and the rectangular resonator height. With the increase of the rectangular resonator height, FR_1 and FR_2 produce redshifts from 710 to 735 nm and from 1235 to 1325 nm, respectively. Transmission spectra of the plasmonic structure with different outer radii of the quarter-ring resonator are shown in Fig. 7a. With the increase of the outer radius, the transmittance of the Fano resonances gradually decreases. Meanwhile, FR_1 and FR_2 produce obvious redshifts from 700 to 755 nm and from 1225 to 1340 nm respectively, and the shift of FR_2 is also greater than that of FR_1, as shown in Fig. 7b.

Next, we investigate the refractive index sensing based on the effects of the refractive index of the r-shaped resonator on the resonance wavelengths. Generally, sensitivity (S) and FOM are crucial parameters for assessing the performances of sensors, which are defined as:

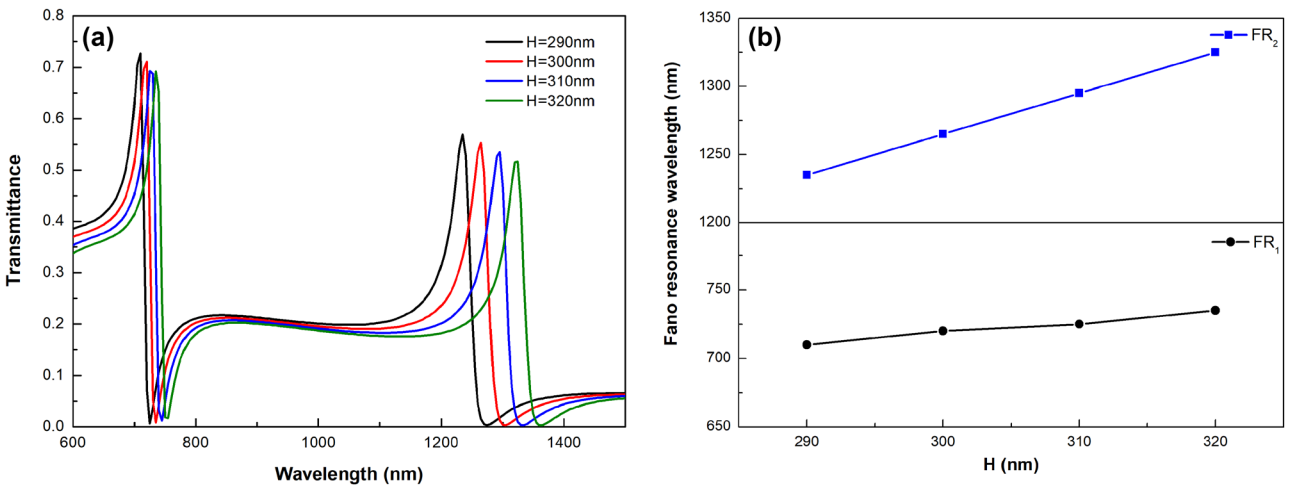

Fig. 6 **a** Transmission spectra of the plasmonic structure with different rectangular resonator height. **b** Relationship between the Fano resonance wavelength and the rectangular resonator height

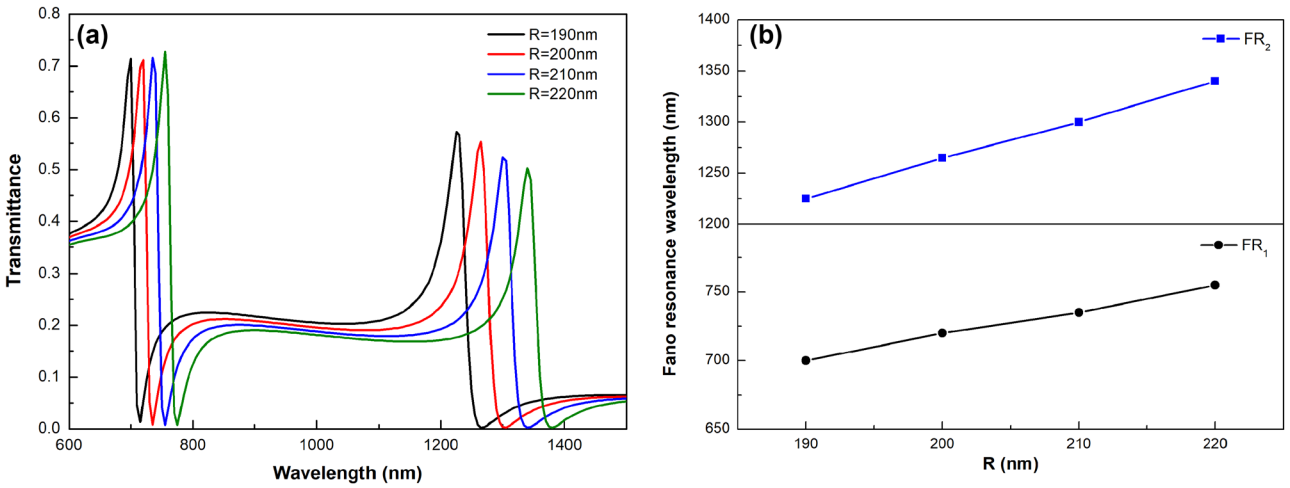

Fig. 7 **a** Transmission spectra of the plasmonic structure with different outer radii. **b** Relationship between the Fano resonance wavelength and the outer radius

$$S = \frac{\Delta\lambda}{\Delta n}, \tag{3}$$

$$FOM = \frac{\Delta T}{T\Delta n}, \tag{4}$$

where $\Delta\lambda$ is the resonance wavelength shift, Δn is the change of the refractive index, T is the transmittance, and ΔT is the transmittance change induced by Δn at a fixed wavelength [36].

The transmission spectra of the plasmonic structure with different refractive indices are shown in Fig. 8a, where the refractive index varies from 1.00 to 1.12 with an interval of 0.03 and other parameters are set as $R = 200$ nm, $R_0 = 150$ nm, $H = 300$ nm, $S = 10$ nm, and $g = 10$ nm. It can be seen that the Fano resonance wavelengths exhibit significant redshifts with the increase of the refractive index, and the shift of FR_1 is smaller than that of FR_2. Figure 8b shows the approximately linear relationships between the Fano resonance wavelengths and the refractive index. The good linearity of FR_1 and FR_2 is of great importance for a high-performance sensor. Here, the slope of the straight line represents the sensitivity. Thus, the sensitivities of the refractive index sensing are about 667 nm/RIU for FR_1 and 1250 nm/RIU for FR_2, respectively.

Moreover, we investigate the effects of the coupling distance, the baffle width, the rectangular resonator height, and the outer radius of the quarter-ring resonator on sensitivity.

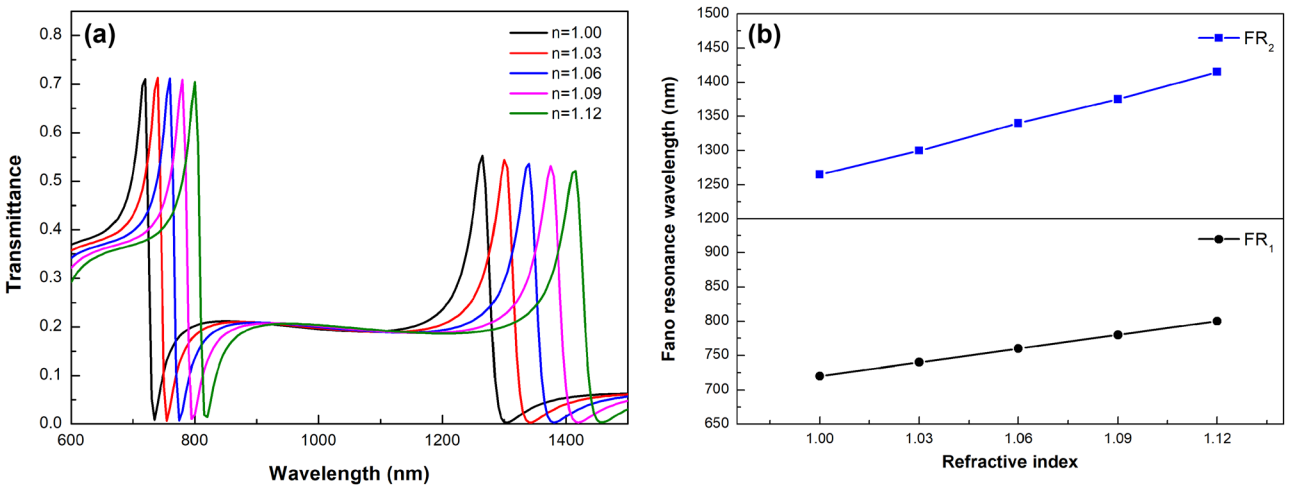

Fig. 8 **a** Transmission spectra of the plasmonic structure with different refractive indices. **b** Relationship between the Fano resonance wavelength and the refractive index

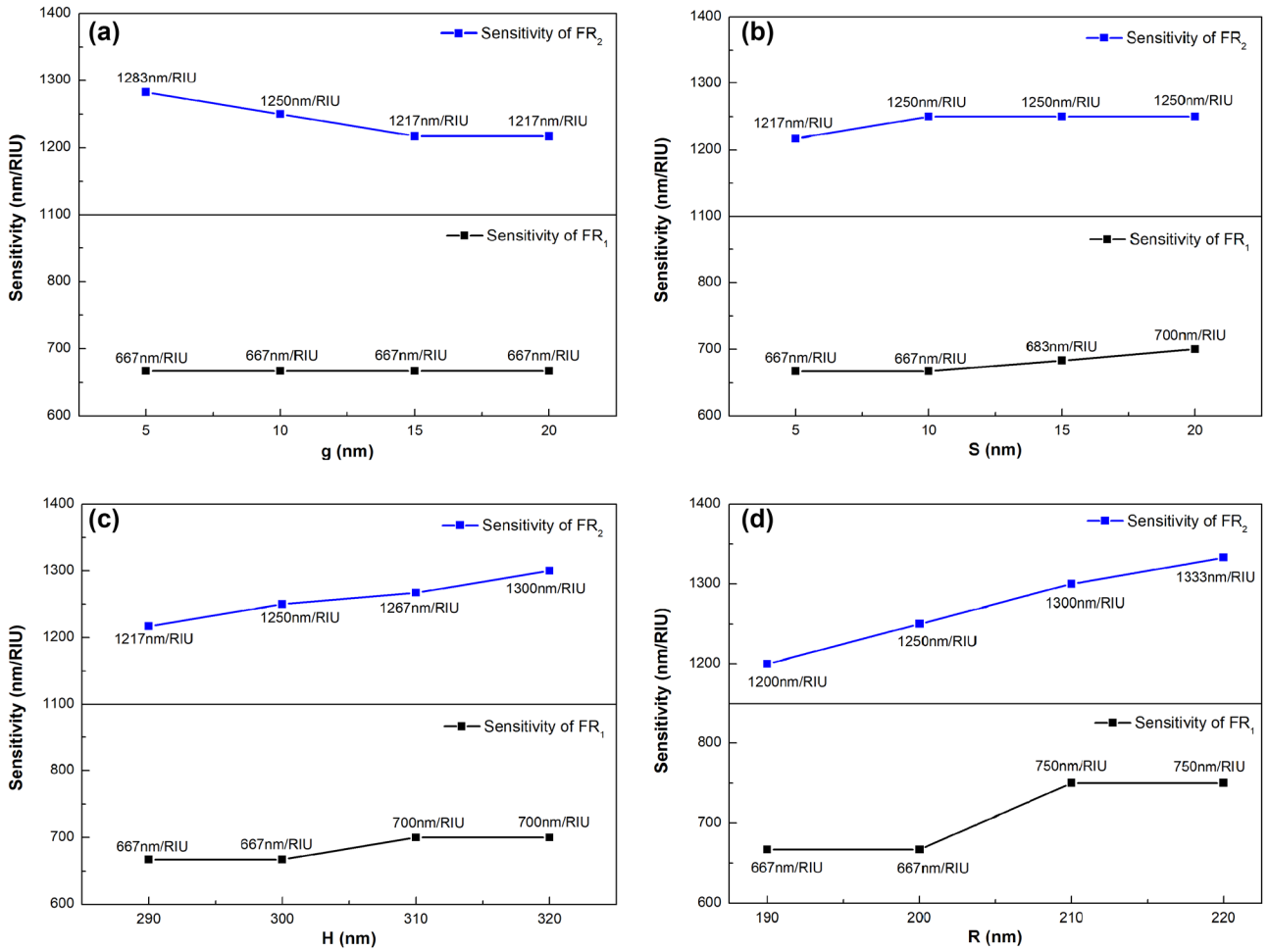

Fig. 9 Sensitivities of the plasmonic structure with different geometrical parameters. **a** The coupling distance, **b** the baffle width, **c** the rectangular resonator height, and **d** the outer radius of the quarter-ring resonator

The surrounding refractive index is increased from 1.00 to 1.12 with an interval of 0.03. Sensitivities of the plasmonic structure with different geometrical parameters are shown in Fig. 9. It can be seen that the geometrical parameters have different effects on sensitivity as described in Fig. 9a–d. The changes of geometrical parameters can affect the transmission characteristics of the structure and then adjust the sensing performances. By optimizing the geometrical parameters, we can achieve the maximum sensitivity of 1333 nm/RIU. Figure 10 shows the FOM of the plasmonic structure, and the surrounding refractive index is increased from 1.00 to 1.12 with an interval of 0.03. The maximum FOM is about 5876. The comparison of the sensitivity and FOM of this paper with other published papers is presented in Table 1.

Based on the refractive index sensing, the plasmonic structure can also be used to measure the biological parameters that can affect the refractive index of the waveguide, such as glucose concentration, glycerin concentration, and plasma concentration, in a much more exact and efficient manner due to the ability to detect small changes in refractive index [40]. The refractive index has unique characteristics for each

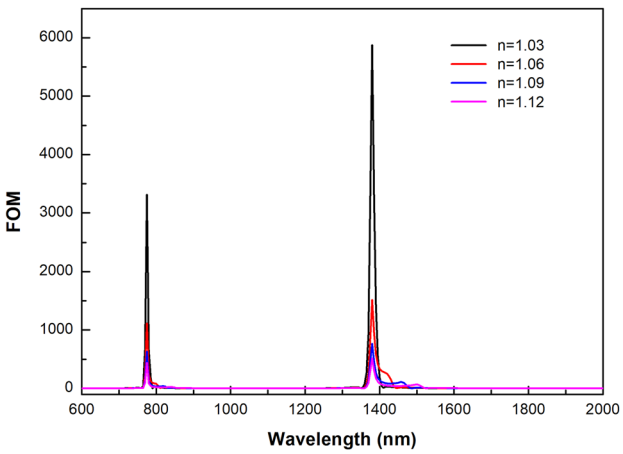

Fig. 10 FOM for different refractive indices

Table 1 Comparison of the sensitivity and FOM with other published papers

Structure	Sensitivity	FOM	Reference
MIM waveguide coupled with rectangular and ring resonators	1125 nm/RIU	75	[37]
MIM waveguide coupled with tangent-ring resonators	880 nm/RIU	964	[38]
MIM waveguide with a baffle and a circular split-ring resonator cavity	1114.3 nm/RIU	55.71	[20]
MIM waveguide structures consist of a cross-shaped cavity and baffle	1100 nm/RIU	9.95×10^4	[39]
MIM waveguide system with asymmetric X-shaped resonant cavity	1303 nm/RIU	3113	[10]
MIM waveguide with an r-shaped resonator	1333 nm/RIU	5876	This paper

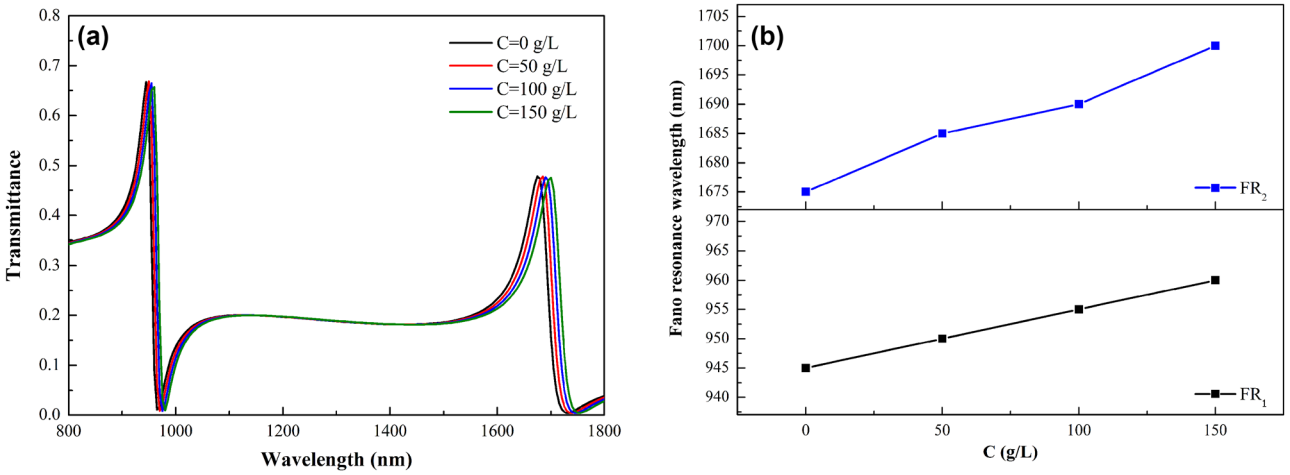

Fig. 11 **a** Transmission spectra of the structure with different glucose solution concentrations. **b** Relationship between the Fano resonance wavelength and the glucose solution concentration

material, and here we discuss the sensing of glucose solution concentration. The refractive index of glucose solution is described as [41] :

$$n = 0.00011889\mathrm{C} + 1.33230545 \quad (5)$$

where C is the concentration of glucose solution. It can be seen that there is a linear relationship between the refractive index and the concentration of glucose.

The transmission spectra of the structure with different glucose solution concentrations are shown in Fig. 11a, where the concentration of glucose solution in the r-shaped resonator is increased from 0 to 150 g/L with an interval of 50 g/L. The glucose solution concentration can affect the Fano resonance wavelengths by changing the refractive index, and the resonance wavelengths of the two Fano resonances exhibit redshifts. Figure 11b shows the relationships between the resonance wavelengths and the concentration of glucose solution. The sensitivity of glucose solution concentration sensing is $S_{glucose} = \Delta\lambda/\Delta\mathrm{C}$. Thus, the sensitivities of FR_1 and FR_2 are about 0.1 nm·L/g and 0.16 nm·L/g, respectively.

Conclusion

In this paper, we propose a plasmonic structure of MIM waveguide consisting of a baffle waveguide and an r-shaped resonator to produce Fano resonance and investigate its Fano transmission characteristics by using the FEM. Two Fano resonances can be produced and tuned by changing the geometrical parameters of the structure. The geometrical parameters can affect the sensitivity of refractive index sensing, and the maximum sensitivity is 1333 nm/RIU with the FOM of 5876. The application of the structure in glucose solution concentration sensing is also investigated, and the maximum sensitivity is about 0.16 nm·L/g. Based on the results, the structure may have potential applications in refractive index nano-sensing, bio-sensing, and nanophotonic devices.

Author Contribution Siti Rohimah has contributed to conceptualization, design, analysis, writing, review, and editing. He Tian has contributed to supervision, funding acquisition, review, and editing manuscript. Jinfang Wang, Jianfeng Chen, Jina Li, Xing Liu, Jingang

Cui, Qiang Xu, and Yu Hao contributed to validating and editing the manuscript. All authors have read and agreed to the published version of the manuscript.

Funding This work was supported in part by the Fundamental Research Funds for the Central Universities (No. 2572019BC04) and in part by the Heilongjiang Provincial Natural Science Foundation of China (No. LH2019F041).

Availability of Data and Materials Not applicable.

Code Availability Not applicable.

Declarations

Ethics Approval Not applicable.

Consent to Participle Not applicable.

Consent for Publication The manuscript has not been published before and is not being considered for publication elsewhere. All authors have contributed to the manuscript creation and read and approved the final manuscript.

Conflict of Interest The authors declare no competing interests.

References

1. Barnes WL, Dereux A, Ebbesen TW (2003) Surface plasmon subwavelength optics. Nature 424(6950):824–830. https://doi.org/10.1038/nature01937
2. Bochenkov VE, Frederiksen M, Sutherland DS (2013) Enhanced refractive index sensitivity of elevated short-range ordered nanohole arrays in optically thin plasmonic Au films. Opt Express 21(12):14763–14770. https://doi.org/10.1364/OE.21.014763
3. Schuller JA, Barnard ES, Cai W, Jun YC, White JS, Brongersma ML (2010) Plasmonics for extreme light concentration and manipulation. Nat Mater 9(3):193–204. https://doi.org/10.1038/nmat2630
4. Yang S, Yu D, Liu G, Lin Q, Zhai X, Wang L (2018) Perfect plasmon-induced absorption and its application for multi-switching in simple plasmonic system. Plasmonics 13(3):1015–1020. https://doi.org/10.1007/s11468-017-0599-9
5. Shahamat Y, Vahedi M (2019) Mid-infrared plasmonically induced absorption and transparency in a Si-based structure for temperature sensing and switching applications. Opt Commun 430:227–233. https://doi.org/10.1016/j.optcom.2018.08.047
6. Chen J, Sun C, Gong Q (2014) Fano resonances in a single defect nanocavity coupled with a plasmonic waveguide. Opt Lett 39(1):52–55. https://doi.org/10.1364/OL.39.000052
7. Chen Z, Cui L, Song X, Yu L, Xiao J (2015) High sensitivity plasmonic sensing based on Fano interference in a rectangular ring waveguide. Opt Commun 340:1–4. https://doi.org/10.1016/j.optcom.2014.11.081
8. Pang S, Huo Y, Xie Y, Hao L (2017) Tunable electromagnetically induced transparency-like in plasmonic stub waveguide with cross resonator. Plasmonics 12(4):1161–1168. https://doi.org/10.1007/s11468-016-0371-6
9. Xiao G, Xu Y, Yang H, Ou Z, Chen J, Li H, Liu X, Zeng L, Li J (2021) High sensitivity plasmonic sensor based on Fano resonance with inverted U-shaped resonator. Sensors 21(4):1164. https://doi.org/10.3390/s21041164
10. Li J, Chen J, Liu X, Tian H, Wang J, Cui J, Rohimah S (2021) Optical sensing based on multimode Fano resonances in metal-insulator-metal waveguide systems with X-shaped resonant cavities. Appl Opt 60(18):5312–5319. https://doi.org/10.1364/AO.427862
11. Chen Z, Segev M (2021) Highlighting photonics: looking into the next decade. eLight 1:2. https://doi.org/10.1186/s43593-021-00002-y
12. Rohimah S, Tian H, Wang J, Chen J, Li J, Liu X, Cui J, Hao Y (2022) Tunable multiple Fano resonances based on a plasmonic metal-insulator-metal structure for nano-sensing and plasma blood sensing applications. Appl Opt 61(6):1275–1283. https://doi.org/10.1364/AO.450084
13. Rahimzadegan A, Granpayeh N, Hosseini SP (2014) Improved plasmonic filter, ultra-compact demultiplexer, and splitter. J Opt Soc Korea 18(3):261–273. https://doi.org/10.3807/JOSK.2014.18.3.261
14. Khani S, Danaie M, Rezaei P (2019) Design of a single-mode plasmonic bandpass filter using a hexagonal resonator coupled to graded-stub waveguides. Plasmonics 14(1):53–62. https://doi.org/10.1007/s11468-018-0777-4
15. Jankovic N, Cselyuszka N (2019) High-resolution plasmonic filter and refractive index sensor based on perturbed square cavity with slits and orthogonal feeding scheme. Plasmonics 14(3):555–560. https://doi.org/10.1007/s11468-018-0834-z
16. Veronis G, Fan S (2007) Theoretical investigation of compact couplers between dielectric slab waveguides and two-dimensional metal-dielectric-metal plasmonic waveguides. Opt Express 15(3):1211–1221. https://doi.org/10.1364/OE.15.001211
17. Bian Y, Zheng Z, Liu Y, Liu J, Zhu J, Zhou T (2011) Hybrid wedge plasmon polariton waveguide with good fabrication-error-tolerance for ultra-deep-subwavelength mode confinement. Opt Express 19(23):22417–22422. https://doi.org/10.1364/OE.19.022417
18. Jeong C, Kim M, Kim S (2013) Circular hybrid plasmonic waveguide with ultra-long propagation distance. Opt Express 21(14):17404–17412. https://doi.org/10.1364/OE.21.017404
19. Ren X, Ren K, Cai Y (2017) Tunable compact nanosensor based on Fano resonance in a plasmonic waveguide system. Appl Opt 56(31):H1–H9. https://doi.org/10.1364/AO.56.0000H1
20. Wang M, Zhang M, Wang Y, Zhao R, Yan S (2019) Fano resonance in an asymmetric MIM waveguide structure and its application in a refractive index nanosensor. Sensors 19(4):791. https://doi.org/10.3390/s19040791
21. Luk'yanchuk B, Zheludev NI, Maier SA, Halas NJ, Nordlander P, Giessen H, Chong CT, (2010) The Fano resonance in plasmonic nanostructures and metamaterials. Nat Mater 9(9):707–715. https://doi.org/10.1038/NMAT2810
22. Miroshnichenko AE, Flach S, Kivshar YS (2010) Fano resonances in nanoscale structures. Rev Mod Phys 82(3):2257–2298. https://doi.org/10.1103/RevModPhys.82.2257
23. Butet J, Martin OJF (2014) Fano resonances in the nonlinear optical response of coupled plasmonic nanostructures. Opt Express 22(24):29693–29707. https://doi.org/10.1364/OE.22.029693
24. Chen J, Li Z, Zhang X, Xiao J, Gong Q (2013) Submicron bidirectional all-optical plasmonic switches. Sci Rep 3:1451. https://doi.org/10.1038/srep01451
25. Chen J, Li J, Liu X, Rohimah S, Tian H, Qi D (2021) Fano resonance in a MIM waveguide with double symmetric rectangular stubs and its sensing characteristics. Opt Commun 482:126563. https://doi.org/10.1016/j.optcom.2020.126563
26. Liu X, Li J, Chen J, Rohimah S, Tian H, Wang J (2021) Independently tunable triple Fano resonances based on MIM waveguide structure with a semi-ring cavity and its sensing characteristics. Opt Express 29(13):20829–20838. https://doi.org/10.1364/OE.428355
27. Gai H, Wang J, Tian Q (2007) Modified Debye model parameters of metals applicable for broadband calculations. Appl Opt 46(12):2229–2233. https://doi.org/10.1364/AO.46.002229

28. Lu H, Liu X, Mao D, Gong Y, Wang G (2011) Induced transparency in nanoscale plasmonic resonator systems. Opt Lett 36(16):3233–3235. https://doi.org/10.1364/OL.36.003233
29. Niu X, Hu X, Chu S, Gong Q (2018) Epsilon-near-zero photonics: a new platform for integrated devices. Adv Opt Mater 6(10):1701292. https://doi.org/10.1002/adom.201701292
30. Lee D, So S, Hu G, Kim M, Badloe T, Cho H, Kim J, Kim H, Qiu C, Rho J (2022) Hyperbolic metamaterials: fusing artificial structures to natural 2D materials. eLight 2:1. https://doi.org/10.1186/s43593-021-00008-6
31. Zhang Q, Huang X, Lin X, Tao J, Jin X (2009) A subwavelength coupler-type MIM optical filter. Opt Express 17(9):7549–7554. https://doi.org/10.1364/OE.17.007549
32. Li Z, Wen K, Chen L, Lei L, Zhou J, Zhou D, Fang Y, Wu B (2019) Refractive index sensor based on multiple Fano resonances in a plasmonic MIM structure. Appl Opt 58(18):4878–4883. https://doi.org/10.1364/AO.58.004878
33. Hu F, Yi H, Zhou Z (2011) Band-pass plasmonic slot filter with band selection and spectrally splitting capabilities. Opt Express 19(6):4848–4855. https://doi.org/10.1364/OE.19.004848
34. Fang Y, Wen K, Qin Y, Li Z, Wu B (2019) Multiple Fano resonances in an end-coupled MIM waveguide system. Opt Commun 452:12–17. https://doi.org/10.1016/j.optcom.2019.06.076
35. Liu X, Li J, Chen J, Rohimah S, Tian H, Wang J (2020) Fano resonance based on D-shaped waveguide structure and its application for human hemoglobin detection. Appl Opt 59(21):6424–6430. https://doi.org/10.1364/AO.397976
36. Yun B, Hu G, Zhang R, Cui Y (2016) Fano resonances in a plasmonic waveguide system composed of stub coupled with a square cavity resonator. J Opt 18(5):055002. https://doi.org/10.1088/2040-8978/18/5/055002
37. Tang Y, Zhang Z, Wang R, Hai Z, Xue C, Zhang W, Yan S (2017) Refractive index sensor based on Fano resonances in metal-insulator-metal waveguides coupled with resonators. Sensors 17(4):784. https://doi.org/10.3390/s17040784
38. Guo Z, Wen K, Hu Q, Lai W, Lin J, Fang Y (2018) Plasmonic multichannel refractive index sensor based on subwavelength tangent-ring metal–insulator–metal waveguide. Sensors 18(5):1348. https://doi.org/10.3390/s18051348
39. Yang Q, Liu X, Guo F, Bai H, Zhang B, Li X, Tan Y, Zhang Z (2020) Multiple Fano resonance in MIM waveguide system with cross-shaped cavity. Optik 220:165163. https://doi.org/10.1016/j.ijleo.2020.165163
40. Wang M, Tian H, Liu X, Li J, Liu Y (2022) Multiparameter sensing based on tunable Fano resonances in MIM waveguide structure with square-ring and triangular cavities. Photonics 9(5):291. https://doi.org/10.3390/photonics9050291
41. Yeh Y (2008) Real-time measurement of glucose concentration and average refractive index using a laser interferometer. Opt Lasers Eng 46(9):666–670. https://doi.org/10.1016/j.optlaseng.2008.04.008